

# UAV-Aided Wireless Communication Designs With Propulsion Energy Limitations

Subin Eom, Hoon Lee, Junhee Park and Inkyu Lee, *Fellow, IEEE*

School of Electrical Eng., Korea University, Seoul, Korea

Email: {esb777, ihun1, pjh0585, inkyu}@korea.ac.kr

## Abstract

This paper studies unmanned aerial vehicle (UAV) aided wireless communication systems where a UAV supports uplink communications of multiple ground nodes (GNs) while flying over the area of the interest. In this system, the propulsion energy consumption at the UAV is taken into account so that the UAV's velocity and acceleration should not exceed a certain threshold. We formulate the minimum average rate maximization problem and the energy efficiency (EE) maximization problem by jointly optimizing the trajectory, velocity, and acceleration of the UAV and the uplink transmit power at the GNs. As these problems are non-convex in general, we employ the successive convex approximation (SCA) techniques. To this end, proper convex approximations for the non-convex constraints are derived, and iterative algorithms are proposed which converge to a local optimal point. Numerical results demonstrate that the proposed algorithms outperform baseline schemes for both problems. Especially for the EE maximization problem, the proposed algorithm exhibits about 109 % gain over the baseline scheme.

## I. INTRODUCTION

Recently, unmanned aerial vehicles (UAVs) have received great attentions as a new communication entity in wireless networks [1]. Compared to conventional terrestrial communications where users are served by ground base stations (BSs) fixed at given position [2], UAV-aided systems could be dispatched to the field with various purposes such as disaster situations and military uses. Moreover, located high above users, UAVs are likely to have line-of-sight (LoS) communication links for air-to-ground channels.

Utilizing these advantages, UAVs have been considered to diverse wireless communication systems. The authors in [3] and [4] studied a mobile relaying system where a UAV helps the communication of ground nodes (GNs) without direct communication links. In this UAV-aided

relaying system, compared to conventional static relay schemes [5], [6], the UAV can move closer to source and destination nodes in order to obtain good channel conditions, and thus the system throughput can be significantly improved. In [3], the throughput of mobile relaying channels was maximized by optimizing the transmit power at the source and the relay node as well as the trajectory of the mobile relay. For the fixed relay trajectory, the work [4] addressed the secrecy rate maximization problem for the UAV-based relaying system with an external eavesdropper.

In addition, UAVs have been adopted to assist conventional terrestrial communication infrastructures [7]–[9]. For the disaster situation, UAVs were employed in [7] to recover malfunctioned ground infrastructure. The work in [8] examined a system where the UAV serves cell-edge users by jointly optimizing UAV's trajectory, bandwidth allocation, and user partitioning. Also, the flying computing cloudlets with UAVs were introduced to provide the offloading opportunities to multiple users [9].

Moreover, the UAVs could play the role of mobile BSs in wireless networks [10]–[12]. The authors in [10] derived mathematical expressions for the optimum altitude of the UAVs that maximizes the coverage of the cellular network. Also, the trajectory optimization methods for mobile BSs were presented in [11] and [12]. Assuming that the GNs are located in a line, the minimum throughput performance was maximized in [11] by optimizing the position of a UAV on a straight line. This result was extended in [12] to a general scenario where multiple UAVs fly three-dimensional space to communicate with GNs. The joint optimization algorithms for the UAV trajectory, transmit power, and time allocation were provided in [12] to maximize the minimum throughput performance. However, these works did not consider the propulsion energy consumption of the UAVs necessary for practical UAV designs under limited on-board energy situation [13].

By taking this issue into account, recent works [14]–[16] investigated energy efficiency (EE) of the UAV system. Different from conventional systems which consider only communication-related energy consumption [17]–[19], the EE of the UAV should address the propulsion energy at the UAV additionally. The authors in [14] maximized the EE by controlling the turning radius of a UAV for mobile relay systems. Also, by jointly optimizing the time allocation, speed, and trajectory, both the spectrum efficiency and the EE were maximized in [15]. In [16], the propulsion energy consumption of the UAV was theoretically modeled, and the EE of the UAV was maximized for a single GN system.

This paper studies UAV-aided wireless communications where a UAV with limited propulsion

energy receives the data of multiple GNs in the uplink. It is assumed that all GNs and the UAV operate in the same frequency band and there are no direct communication links among GNs. Under these setup, we formulate the minimum rate maximization problem and the EE maximization problem by jointly optimizing the UAV trajectory, the velocity, the acceleration, and the uplink transmit power at the GNs. A similar approach for solving the minimum rate maximization was studied in [12], but the authors in [12] did not involve the propulsion energy consumption at the UAV. For the EE maximization problem, our work can be regarded as a generalization of the single GN system in [16] to the multi-GN scenario, and thus we need to deal with inter-node interference as well. Due to these issues, existing algorithms presented in [12] and [16] cannot be directly applied to our problems.

To tackle our problem of interest, we introduce auxiliary variables which couple the trajectory variables and the uplink transmit power in order to jointly optimize these variables. As the equivalent problem is still non-convex, we employ the successive convex approximation (SCA) technique which successively solves approximated convex problems of the original non-convex one. In order to apply the SCA to our optimization problems, we present new convex surrogate functions for the non-convex constraints. Then, we propose efficient algorithms for the minimum rate maximization problem and the EE maximization problem which yield local optimal solutions. Simulation results confirm that the proposed algorithms provide a significant performance gain over baseline schemes.

The rest of this paper is organized as follows: Section II explains the system model and the problem formulations for the UAV-aided communication systems. In Section III, the minimum rate maximization and the EE maximization algorithms are proposed. We examine the circular trajectory case as baseline schemes in Section IV. Section V presents the numerical results for the proposed algorithms and we conclude the paper in Section VI.

*Notations:* Throughout this paper, the bold lower-case and normal letters denote vectors and scalars, respectively. The space of  $M$ -dimensional real-valued vectors are represented by  $\mathbb{R}^{M \times 1}$ . For a vector  $\mathbf{a}$ ,  $\|\mathbf{a}\|$  and  $\mathbf{a}^T$  indicate norm and transpose, respectively. The gradient of a function  $f$  is defined as  $\nabla f$ . For a time-dependent function  $\mathbf{x}(t)$ ,  $\dot{\mathbf{x}}(t)$  and  $\ddot{\mathbf{x}}(t)$  stand for the first-order and second-order derivatives with respect to time  $t$ , respectively.

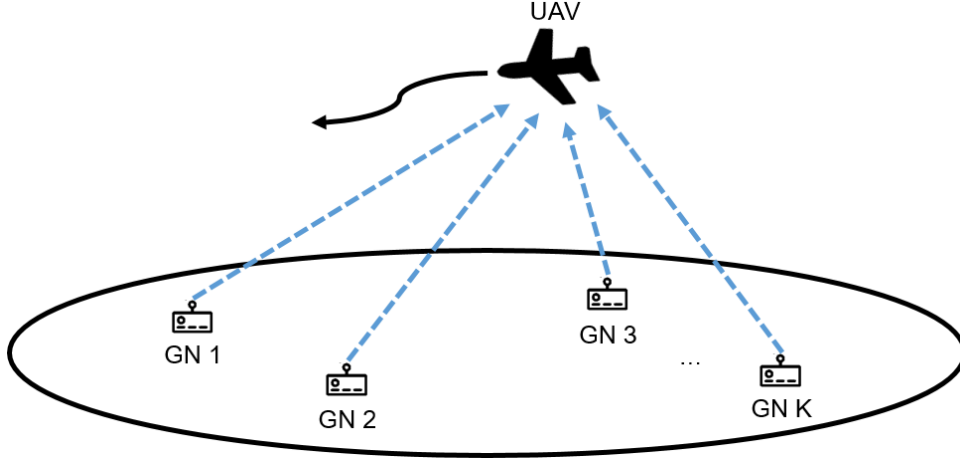


Fig. 1. UAV-enabled wireless network

## II. SYSTEM MODEL AND PROBLEM FORMULATION

As shown in Fig. 1, we consider UAV-aided wireless communications where a UAV receives uplink information transmitted from  $K$  GNs. The UAV horizontally flies at a constant altitude  $H$  with a time period  $T$ , while the GNs are located at fixed positions, which are perfectly known to the UAV in advance. For the location of the GNs and the UAV, we employ a three-dimensional Cartesian coordinate system, and thus the horizontal coordinate of GN  $k$  ( $k = 1, \dots, K$ ) is denoted by  $\mathbf{w}_k = [x_k \ y_k]^T$ . Also, we define the time-varying horizontal coordinate of the UAV at time instant  $t$  as  $\mathbf{q}(t) = [q_x(t) \ q_y(t)]^T$ , for  $0 \leq t \leq T$ . Then, the instantaneous velocity  $\mathbf{v}(t)$  and the acceleration  $\mathbf{a}(t)$  of the UAV are expressed by  $\mathbf{v}(t) \triangleq \dot{\mathbf{q}}(t)$  and  $\mathbf{a}(t) \triangleq \ddot{\mathbf{q}}(t)$ , respectively.

Continuous time expressions of variables make analysis and derivations in the UAV systems intractable. For ease of analysis, we discretize the time duration  $T$  into  $N$  time slots with the same time interval  $\delta_t = \frac{T}{N}$  [3]. As a result, the trajectory of the UAV can be represented by  $N$  vector sequences  $\mathbf{q}[n] \triangleq \mathbf{q}(n\delta_t)$ ,  $\mathbf{v}[n] \triangleq \mathbf{v}(n\delta_t)$ , and  $\mathbf{a}[n] \triangleq \mathbf{a}(n\delta_t)$  for  $n = 0, 1, \dots, N$ . When the discretized time interval  $\delta_t$  is chosen as a small number, the velocity and the acceleration can be approximated by using Taylor expansions as [16]

$$\mathbf{v}[n] = \mathbf{v}[n-1] + \mathbf{a}[n-1]\delta_t, \text{ for } n = 1, \dots, N, \quad (1)$$

$$\mathbf{q}[n] = \mathbf{q}[n-1] + \mathbf{v}[n-1]\delta_t + \frac{1}{2}\mathbf{a}[n-1]\delta_t^2, \text{ for } n = 1, \dots, N. \quad (2)$$

Also, assuming the periodical operation at the UAV, we have [12]

$$\mathbf{q}[0] = \mathbf{q}[N], \mathbf{v}[0] = \mathbf{v}[N], \mathbf{a}[0] = \mathbf{a}[N], \quad (3)$$

which implies that after one period  $T$ , the UAV returns to its starting location with the same velocity and acceleration.

In addition, the acceleration and the velocity of the practical UAV are subject to

$$\|\mathbf{a}[n]\| \leq a_{\max}, \text{ for } n = 0, 1, \dots, N, \quad (4)$$

$$V_{\min} \leq \|\mathbf{v}[n]\| \leq V_{\max}, \text{ for } n = 0, 1, \dots, N, \quad (5)$$

where  $a_{\max}$  indicates the maximum UAV acceleration in  $\text{m/sec}^2$  and  $V_{\min}$  and  $V_{\max}$  stand for the minimum and the maximum UAV speed constraints in  $\text{m/sec}$ , respectively. Notice that the minimum speed constraint  $V_{\min}$  is important for practical fixed-wing UAV designs which need to move forward to remain aloft and thus cannot hover over a fixed location [16].

For the power consumption at the UAV, we take into account the propulsion power utilized for maintaining the UAV aloft and supporting its mobility. The propulsion power of the UAV  $P_{\text{prop}}[n]$  at time slot  $n$  is given by [16]

$$P_{\text{prop}}[n] = c_1 \|\mathbf{v}[n]\|^3 + \frac{c_2}{\|\mathbf{v}[n]\|} \left( 1 + \frac{\|\mathbf{a}[n]\|^2}{g^2} \right), \text{ for } n = 0, 1, \dots, N, \quad (6)$$

where  $c_1$  and  $c_2$  are the parameters related to the aircraft design and  $g = 9.8 \text{ m/sec}^2$  equals the gravitational acceleration. Thus, the average propulsion power and the total consumed propulsion energy over  $N$  time slots are obtained by  $\frac{1}{N} \sum_{n=1}^N P_{\text{prop}}[n]$  and  $\delta_t \sum_{n=1}^N P_{\text{prop}}[n]$ , respectively. The power consumed by signal processing circuits such as analog-to-digital converters and channel decoders are ignored since they are practically much smaller than the propulsion power [16].

Now, let us explain the channel model between the UAV and the GNs. We assume that the air-to-ground communication links are dominated by the LoS links. Moreover, the Doppler effect due to the UAV mobility is assumed to be well compensated. Then, the effective channel gain  $h_k[n]$  from GN  $k$  to the UAV at time slot  $n$  follows the free-space path loss model as [3]

$$h_k[n] = \frac{\gamma_0}{d_k^2[n]}, \quad (7)$$

where  $\gamma_0 \triangleq \beta_0/\sigma^2$  represents the reference signal-to-noise ratio (SNR) at 1 m with  $\beta_0$  and  $\sigma^2$  being the channel power at 1 m and the white Gaussian noise power at the UAV, respectively, and the distance  $d_k[n]$  is written by

$$d_k[n] = \sqrt{\|\mathbf{q}[n] - \mathbf{w}_k\|^2 + H^2}. \quad (8)$$

At time slot  $n$ , GN  $k$  transmits its data signal to the UAV with power  $0 \leq p_k[n] \leq P_{\text{peak}}$ , where  $P_{\text{peak}}$  is the peak transmission power constraint at the GNs. Accordingly, the instantaneous achievable rate  $R_k[n]$  can be expressed as

$$R_k[n] = \log_2 \left( 1 + \frac{p_k[n]h_k[n]}{1 + \sum_{j=1, j \neq k}^K p_j[n]h_j[n]} \right), \quad (9)$$

where the term  $\sum_{j=1, j \neq k}^K p_j[n]h_j[n]$  stands for interference from other GNs. Therefore, the achievable average rate of the GN  $k$  and the total information bits transmitted from GN  $k$  over  $N$  time slots are denoted as  $\frac{1}{N} \sum_{n=1}^N R_k[n]$  and  $W\delta_t \sum_{n=1}^N R_k[n]$ , respectively, where  $W$  means the bandwidth.

In this paper, we jointly optimize the variables  $\mathbf{q}[n]$ ,  $\mathbf{v}[n]$ , and  $\mathbf{a}[n]$  and the uplink transmit power  $p_k[n]$  at the GNs so that the minimum average rate among multiple GNs and the EE are maximized, respectively. First, the minimum rate maximization problem can be formulated as

$$(P1) : \max_{\substack{\{\mathbf{q}[n], \mathbf{v}[n], \mathbf{a}[n]\} \\ \{p_k[n], \tau\}}} \tau \quad (10a)$$

$$s.t. \quad \frac{1}{N} \sum_{n=1}^N R_k[n] \geq \tau, \forall k, \quad (10b)$$

$$0 \leq p_k[n] \leq P_{\text{peak}}, \forall k, n, \quad (10c)$$

$$\frac{1}{N} \sum_{n=1}^N P_{\text{prop}}[n] \leq P_{\text{lim}}, \quad (10d)$$

$$(1) - (5),$$

where  $P_{\text{lim}}$  in (10d) indicates the propulsion power constraint at the UAV.

Next, to support all of the individual GNs, the fairness based EE [20]–[22] is more suitable than the network-wise EE [18], [19]. Thus, we define the EE in the UAV-aided wireless communication systems as the ratio between the minimum information bits transmitted among the GNs and the total energy consumed at the UAV. Therefore, the EE maximization problem can be written by

$$(P2) : \max_{\substack{\{\mathbf{q}[n], \mathbf{v}[n], \mathbf{a}[n]\} \\ \{p_k[n], \eta\}}} \frac{\eta}{\sum_{n=1}^N P_{\text{prop}}[n]} \quad (11a)$$

$$W \sum_{n=1}^N R_k[n] \geq \eta, \forall k, \quad (11b)$$

$$s.t. \quad (1) - (5), (10c).$$

In general, (P1) and (P2) are non-convex problems due to the constraints and the objective functions. Compared to [12], we additionally consider the propulsion power constraint (10d) in the minimum rate maximization problem (P1). Also, note that the EE maximization problem (P2) can be regarded as a generalization of [16] which investigated only a single GN scenario. From these respects, the works in [12] and [16] can be regarded as special cases of our problems (P1) and (P2), respectively. To solve the problems (P1) and (P2), we adopt the SCA framework [23] [24] which iteratively solves approximated convex problems for the original non-convex problems.

### III. PROPOSED ALGORITHM

In this section, we propose iterative algorithms for efficiently solving (P1) and (P2) by applying the SCA method. First, the minimum rate maximization problem (P1) is considered in Section III-A, and then it is followed by the EE maximization problem (P2) in Section III-B.

#### A. Minimum Average Rate Maximization

Applying the change of variables as

$$G_k[n] \triangleq p_k[n]h_k[n] = \frac{p_k[n]\gamma_0}{\|\mathbf{q}[n] - \mathbf{w}_k\|^2 + H^2}, \forall k, n, \quad (12)$$

where  $G_k[n]$  is a new optimization variable, the constraint (10c) becomes  $0 \leq G_k[n] \leq G_{k,\max}[n], \forall k, n$ , where  $G_{k,\max}[n] \triangleq P_{\text{peak}}h_k[n] = \frac{P_{\text{peak}}\gamma_0}{\|\mathbf{q}[n] - \mathbf{w}_k\|^2 + H^2}$ . Then, we can rewrite the achievable rate  $R_k[n]$  in (9) as

$$R_k[n] = \log_2 \left( 1 + \sum_{m=1}^K G_m[n] \right) - \hat{R}_k[n], \quad (13)$$

where  $\hat{R}_k[n] \triangleq \log_2 \left( 1 + \sum_{j=1, j \neq k}^K G_j[n] \right)$ .

By introducing new auxiliary variables  $\{V_1[n]\}$ , (P1) can be recast to

$$(P1.1) : \max_{\substack{\{\mathbf{q}[n], \mathbf{v}[n], \mathbf{a}[n]\} \\ \{G_k[n], V_1[n], \tau\}}} \tau \quad (14a)$$

$$s.t. \quad \frac{1}{N} \sum_{n=1}^N \left( \log_2 \left( 1 + \sum_{m=1}^K G_m[n] \right) - \hat{R}_k[n] \right) \geq \tau, \forall k, \quad (14b)$$

$$0 \leq G_k[n] \leq G_{k,\max}[n], \forall k, n, \quad (14c)$$

$$\frac{1}{N} \sum_{n=1}^N c_1 \|\mathbf{v}[n]\|^3 + \frac{c_2}{V_1[n]} + \frac{c_2 \|\mathbf{a}[n]\|^2}{g^2 V_1[n]} \leq P_{\text{lim}}, \quad (14d)$$

$$V_{\min} \leq V_1[n], \forall n, \quad (14e)$$

$$V_1^2[n] \leq \|\mathbf{v}[n]\|^2, \forall n, \quad (14f)$$

$$\|\mathbf{v}[n]\| \leq V_{\max}, \forall n, \quad (14g)$$

$$(1) - (4).$$

It can be shown that at the optimal point of (P1.1), the inequality constraint in (14f) holds with the equality, since otherwise we can enlarge the feasible region corresponding to (14d) by increasing  $V_1[n]$ . Therefore, we can conclude that (P1.1) is equivalent to (P1). Thanks to the new auxiliary variables  $\{V_1[n]\}$ , constraints (14d) and (14e) now become convex, while (14b), (14c), and (14f) are still non-convex in general.

To address these constraints, we employ the SCA methods. First, it can be checked that constraint (14b) is given by a difference of two concave functions. Hence, the convex surrogate function  $\hat{R}_k^{\text{ub}}[n]$  for  $\hat{R}_k[n]$  can be computed from a first order Taylor approximation as

$$\hat{R}_k^{\text{ub}}[n] \triangleq \hat{\Gamma}_k[n] \sum_{j=1, j \neq k}^K (G_{j,l+1}[n] - G_{j,l}[n]) + \log_2 \left( 1 + \sum_{j=1, j \neq k}^K G_{j,l}[n] \right) \geq \hat{R}_k[n], \quad (15)$$

where  $G_{k,l}[n]$  indicates a solution of  $G_k[n]$  attained at the  $l$ -th iteration of the SCA process and  $\hat{\Gamma}_k[n] \triangleq \log_2 e / (1 + \sum_{j=1, j \neq k}^K G_{j,l}[n])$ . Next, to identify the surrogate functions of (14c) and (14f), we present the following lemmas.

*Lemma 1:* Denoting  $\{\mathbf{q}_l[n]\}$  as a solution for  $\{\mathbf{q}[n]\}$  calculated at the  $l$ -th iteration, the concave surrogate function  $G_{k,\max}^{\text{lb}}[n]$  for  $G_{k,\max}[n]$  can be expressed as

$$\begin{aligned} G_{k,\max}^{\text{lb}}[n] &\triangleq P_{\text{peak}} \gamma_0 \left( -\frac{\|\mathbf{q}_{l+1}[n] - \mathbf{w}_k\|^2}{H^4} + B_k[n] (\mathbf{q}_{l+1}[n] - \mathbf{w}_k)^T (\mathbf{q}_l[n] - \mathbf{w}_k) + C_k[n] \right) \\ &\leq G_{k,\max}[n], \end{aligned} \quad (16)$$



where the constants  $B_k[n]$  and  $C_k[n]$  are respectively given as

$$B_k[n] \triangleq 2 \left( \frac{1}{H^4} - \frac{1}{(\|\mathbf{q}_l[n] - \mathbf{w}_k\|^2 + H^2)^2} \right),$$

$$C_k[n] \triangleq \frac{1}{\|\mathbf{q}_l[n] - \mathbf{w}_k\|^2 + H^2} + \frac{2\|\mathbf{q}_l[n] - \mathbf{w}_k\|^2}{(\|\mathbf{q}_l[n] - \mathbf{w}_k\|^2 + H^2)^2} - \frac{\|\mathbf{q}_l[n] - \mathbf{w}_k\|^2}{H^4}.$$

*Proof:* Please refer to Appendix A. ■

*Lemma 2:* From a solution  $\{\mathbf{v}_l[n]\}$  obtained at the  $l$ -th iteration, the concave surrogate function of  $\|\mathbf{v}_{l+1}[n]\|^2$  can be computed as

$$-\|\mathbf{v}_{l+1}[n]\|^2 + 2\mathbf{v}_l^T (2\mathbf{v}_{l+1}[n] - \mathbf{v}_l[n]) \leq \|\mathbf{v}_{l+1}[n]\|^2. \quad (17)$$

*Proof:* Applying a similar process in Appendix A, we can conclude that the function in (17) satisfies the conditions for a concave surrogate function [23]. ■

With the aid of Lemmas 1 and 2, at the  $(l + 1)$ -th iteration, the non-convex constraints in (14c) and (14f) can be approximated as

$$0 \leq G_k[n] \leq G_{k,\max}^{\text{lb}}[n], \quad (18)$$

$$V_1^2[n] \leq -\|\mathbf{v}_{l+1}[n]\|^2 + 2\mathbf{v}_l^T (2\mathbf{v}_{l+1}[n] - \mathbf{v}_l[n]). \quad (19)$$

As a result, with given solutions  $\{\mathbf{q}_l[n], \mathbf{v}_l[n], G_{k,l}[n]\}$  at the  $l$ -th iteration, we solve the following problem at the  $(l + 1)$ -th iteration of the SCA procedure

$$(P1.2) : \max_{\substack{\{\mathbf{q}_{l+1}[n], \mathbf{v}_{l+1}[n], \mathbf{a}[n]\} \\ \{G_{k,l+1}[n], V_1[n], \tau^{\text{lb}}\}}} \tau^{\text{lb}} \quad (20a)$$

$$s.t. \quad \frac{1}{N} \sum_{n=1}^N \left( \log_2 \left( 1 + \sum_{m=1}^K G_{m,l+1}[n] \right) - \hat{R}_k^{\text{ub}}[n] \right) \geq \tau^{\text{lb}}, \forall k, \quad (20b)$$

$$(1) - (4), (14d), (14e), (14g), (18), (19),$$

where  $\tau^{\text{lb}}$  denotes the lower bound of  $\tau$  in the original problem (P1). Since (P1.2) is a convex problem, it can be optimally solved via existing convex optimization solvers, e.g. CVX [25].

Based on these results, we summarize the proposed iterative procedure in Algorithm 1.

---

**Algorithm 1:** Proposed algorithm for (P1)

---

Initialize  $\{\mathbf{q}_0[n], \mathbf{v}_0[n], G_{k,0}[n]\}, \forall k, n$  and let  $l = 0$ .

**Repeat**

    Compute  $\{\mathbf{q}_{l+1}[n], \mathbf{v}_{l+1}[n], G_{k,l+1}[n]\}$  for (P1.2) with given  $\{\mathbf{q}_l[n], \mathbf{v}_l[n], G_{k,l}[n]\}$ .

    Update  $l \leftarrow l + 1$ .

**Until** Convergence.

Obtain  $p_k[n] = \frac{G_{k,l+1}[n]}{h_{k,l+1}[n]}$ .

---

For the convergence analysis of Algorithm 1, let us define the objective values of (P1) and (P1.2) at the  $l$ -th iteration as  $\tau_l$  and  $\tau_l^{\text{lb}}$ , respectively. Then we can express the relationship

$$\tau_l = \tau_l^{\text{lb}} \leq \tau_{l+1}^{\text{lb}} \leq \tau_{l+1}, \quad (21)$$

where the first equation holds because the surrogate functions in (15), (16), and (17) are tight at the given local points, the second inequality is derived from the non-decreasing property of the optimal solution of (P1.2), and the third inequality follows from the fact that the approximation problem (P1.2) is a lower bound of the original problem (P1).

From (21), we can conclude that the objective value  $\tau$  in (P1) is non-decreasing for every iterations of Algorithm 1. Since the objective value  $\tau$  in (P1) has a finite upper bound value and at given local points, the surrogate functions in (15), (16), and (17) obtain the same gradients as their original functions, it can be verified that Algorithm 1 is guaranteed to converge to at least a local optimal solution for (P1) [23], [24].

### B. Energy Efficiency Maximization

In this subsection, we consider the EE maximization problem (P2). First, by applying (12)-(13), and introducing an auxiliary variable  $\{V_1[n]\}$ , (P2) can be transformed as

$$(P2.1) : \max_{\substack{\{\mathbf{q}[n], \mathbf{v}[n], \mathbf{a}[n]\} \\ \{G_k[n], V_1[n], \eta\}}} \frac{\eta}{\sum_{n=1}^N c_1 \|\mathbf{v}[n]\|^3 + \frac{c_2}{V_1[n]} + \frac{c_2 \|\mathbf{a}[n]\|^2}{g^2 V_1[n]}} \quad (22a)$$

$$s.t. \quad W \sum_{n=1}^N \left( \log_2 \left( 1 + \sum_{m=1}^K G_m[n] \right) - \hat{R}_k[n] \right) \geq \eta, \forall k, \quad (22b)$$

$$(1) - (4), (14c), (14e) - (14g).$$

Similar to (P1.1), we can see that (P2.1) is equivalent to (P2), but (P2.1) is still non-convex due to the constraints in (14c), (14f), and (22b).

To tackle this issue, we can employ the similar SCA process presented in Section III-A. By adopting (15) and Lemmas 1 and 2, a convex approximation of (P2.1) at the  $(l+1)$ -th iteration is given by

$$(P2.2) : \max_{\substack{\{\mathbf{q}_{l+1}[n], \mathbf{v}_{l+1}[n], \mathbf{a}[n]\} \\ \{G_{k,l+1}[n], V_1[n], \eta^{\text{lb}}\}}} \frac{\eta^{\text{lb}}}{\sum_{n=1}^N c_1 \|\mathbf{v}[n]\|^3 + \frac{c_2}{V_1[n]} + \frac{c_2 \|\mathbf{a}[n]\|^2}{g^2 V_1[n]}} \quad (23a)$$

$$s.t. \quad W \sum_{n=1}^N \left( \log_2 \left( 1 + \sum_{m=1}^K G_{m,l+1}[n] \right) - \hat{R}_k^{\text{ub}}[n] \right) \geq \eta^{\text{lb}}, \forall k \quad (23b)$$

$$(1) - (4), (14e), (14g), (18), (19),$$

where  $\eta^{\text{lb}}$  denotes the lower bound of  $\eta$  in the original problem (P2).

It can be shown that (P2.2) is a concave-convex fractional problem, which can be optimally solved via the Dinkelbach's method [26], [27]. Then, denoting  $\mu = \sum_{n=1}^N c_1 \|\mathbf{v}[n]\|^3 + \frac{c_2}{V_1[n]} + \frac{c_2 \|\mathbf{a}[n]\|^2}{g^2 V_1[n]}$  with a given constant  $\lambda_m$ , (P2.2) can be converted to (P2.3) as

$$(P2.3) : \begin{aligned} & \max_{\substack{\{\mathbf{q}_{l+1}[n], \mathbf{v}_{l+1}[n], \mathbf{a}[n]\} \\ \{G_{k,l+1}[n], V_1[n], \eta^{\text{lb}}\}}} & \eta^{\text{lb}} - \lambda_m \mu & (24a) \\ & s.t. & (1) - (4), (14e), (14g), (18), (19), (23b). \end{aligned}$$

Based on (P2.3), we summarize the proposed iterative procedure in Algorithm 2. The convergence and the local optimality of Algorithm 2 can be verified similar to Algorithm 1, and thus the details are omitted for brevity.

---

**Algorithm 2:** Proposed algorithm for (P2)

---

Initialize  $\{\mathbf{q}_0[n], \mathbf{v}_0[n], G_{k,0}[n]\}, \forall k, n$  and let  $\lambda_0 = 0, m = 0$ , and  $l = 0$ .

**Repeat**

**Repeat**

Compute  $\{\mathbf{q}_{l+1}[n], \mathbf{v}_{l+1}[n], G_{k,l+1}[n]\}$  for (P2.3) with given

$\{\mathbf{q}_l[n], \mathbf{v}_l[n], G_{k,l}[n]\}, \forall k, n$  and  $\lambda_m$ .

Update  $l \leftarrow l + 1$ .

**Until Convergence.**

Let  $F(\lambda_m) = \eta^{\text{lb}} - \lambda_m \mu$  and  $\lambda_{m+1} = \eta^{\text{lb}} / \mu$ .

Update  $m \leftarrow m + 1$ .

Let  $\{\mathbf{q}_0[n], \mathbf{v}_0[n], G_{k,0}[n]\} = \{\mathbf{q}_{l+1}[n], \mathbf{v}_{l+1}[n], G_{k,l+1}[n]\}, \forall k, n$  and  $l = 0$ .

**Until Convergence.**

Obtain  $p_k[n] = \frac{G_{k,l+1}[n]}{h_{k,l+1}[n]}, \forall k, n$ .

---

It is worthwhile to note that we need to initialize the trajectory variables  $\{\mathbf{q}[n], \mathbf{v}[n]\}$  for (P1) and (P2). However, it is not trivial to find such variables satisfying the UAV movement constraints (1)-(5) and the propulsion power constraint (10d). This will be clearly explained in Section IV-C.

#### IV. CIRCULAR TRAJECTORY SYSTEM

Now, we examine the circular trajectory system which will be used as a baseline scheme. First, we choose the center of the circular trajectory  $\mathbf{c} = [x_0 \ y_0]^T$  as the geometrical mean of the GNs  $\mathbf{c} = \frac{\sum_{k=1}^K \mathbf{w}_k}{K}$ . Denoting  $r$  as the radius of the trajectory and  $\theta[n]$  as the angle of the circle along which the UAV flies at time slot  $n$ , the horizontal coordinate of the UAV  $\mathbf{q}[n]$  can be obtained by  $\mathbf{q}[n] = [r \cos \theta[n] + x_0 \ r \sin \theta[n] + y_0]^T$ . Also, the location of GN  $k$   $\mathbf{w}_k$  can be

represented as  $\mathbf{w}_k = [\zeta_k \cos \varphi_k + x_0 \quad \zeta_k \sin \varphi_k + y_0]^T$ , where  $\zeta_k$  and  $\varphi_k$  equal the distance and the angle between the geometric center  $\mathbf{c}$  and GN  $k$ , respectively. Thus, the distance  $d_k[n]$  between the UAV and GN  $k$  in (8) can be expressed as  $d_k[n] = \sqrt{r^2 + \zeta_k^2 + H^2 - 2r\zeta_k \cos(\theta[n] - \varphi_k)}$ .

By adopting the angular velocity  $\omega[n]$  and the angular acceleration  $\alpha[n]$ , equations in (1)-(6) can be rewritten as

$$\omega[n] = \omega[n-1] + \alpha[n-1]\delta_t, \text{ for } n = 1, \dots, N, \quad (25)$$

$$\theta[n] = \theta[n-1] + \omega[n-1]\delta_t + \frac{1}{2}\alpha[n-1]\delta_t^2, \text{ for } n = 1, \dots, N, \quad (26)$$

$$\theta[N] = \theta[0] + 2\pi, \omega[0] = \omega[N], \alpha[0] = \alpha[N], \quad (27)$$

$$\|\mathbf{a}[n]\|^2 = \|\mathbf{a}_{\parallel}[n]\|^2 + \|\mathbf{a}_{\perp}[n]\|^2 = r^2\alpha^2[n] + r^2\omega^4[n] \leq a_{\max}^2, \text{ for } n = 0, 1, \dots, N, \quad (28)$$

$$\omega_{\min} \leq \omega[n] \leq \omega_{\max}, \text{ for } n = 0, 1, \dots, N, \quad (29)$$

$$P_{\text{prop}}[n] = c_1 r^3 \omega^3[n] + \frac{c_2}{r\omega[n]} + \frac{c_2 r \omega^3[n]}{g^2} + \frac{c_2 r \alpha^2[n]}{g^2 \omega[n]}, \text{ for } n = 0, 1, \dots, N, \quad (30)$$

where  $\mathbf{a}_{\parallel}[n]$  and  $\mathbf{a}_{\perp}[n]$  are the tangential and centripetal accelerations, respectively, and  $\omega_{\min} \triangleq V_{\min}/r$  and  $\omega_{\max} \triangleq V_{\max}/r$  indicate the minimum and maximum angular velocity, respectively.

Similar to Section III, we address the minimum average rate maximization problem and the EE maximization problem for the circular trajectory, which are respectively formulated as

$$(P3) : \max_{\substack{\{\theta[n], \omega[n], \alpha[n]\} \\ \{r, p_k[n], \tau\}}} \tau \quad (31a)$$

$$s.t. \quad r_{\min} \leq r \leq r_{\max}, \quad (31b)$$

$$(10b) - (10d), (25) - (29),$$

$$(P4) : \max_{\substack{\{\theta[n], \omega[n], \alpha[n]\} \\ \{r, p_k[n], \eta\}}} \frac{\eta}{\sum_{n=1}^N P_{\text{prop}}[n]} \quad (32a)$$

$$s.t. \quad (10c), (11b), (25) - (29), (31b),$$

where  $r_{\min} \triangleq \frac{V_{\min} T}{2\pi}$  and  $r_{\max} \triangleq \min\left(\frac{V_{\max} T}{2\pi}, \frac{a_{\max}}{\max(\sqrt{\omega^4[n] + \alpha^2[n]})}\right)$  denote the minimum and maximum radius of the circular trajectory, respectively. It is emphasized that (P3) and (P4) are difficult to solve because of the non-convex constraints and objective functions. To deal with the problems (P3) and (P4), similar SCA frameworks in Section III are applied.

### A. Minimum Average Rate Maximization and EE maximization

For the minimum average rate maximization problem (P3), we first find  $\{r, p_k[n]\}$  with given  $\{\theta[n], \omega[n], \alpha[n]\}$  and then updates  $\{\theta[n], \omega[n], \alpha[n], p_k[n]\}$  for a fixed  $r$ . For given  $\{\theta[n], \omega[n], \alpha[n]\}$ , we adopt the change of variable  $S_k[n]$  and  $S_{k,\max}[n]$  as

$$S_k[n] \triangleq p_k[n] h_k[n] = \frac{p_k[n] \gamma_0}{(r - \zeta_k \cos(\theta[n] - \theta_k))^2 + \zeta_k^2 \sin^2(\theta[n] - \theta_k) + H^2}, \quad (33)$$

$$S_{k,\max}[n] \triangleq P_{\text{peak}} h_k[n] = \frac{P_{\text{peak}} \gamma_0}{(r - \zeta_k \cos(\theta[n] - \theta_k))^2 + \zeta_k^2 \sin^2(\theta[n] - \theta_k) + H^2}. \quad (34)$$

Similar to the method in Section III-A, we employ the SCA to  $S_{k,\max}[n]$ . Based on Lemma 1, the concave surrogate function  $S_{k,\max}^{\text{lb1}}[n]$  of  $S_{k,\max}[n]$  with a solution  $r_l$  at the  $l$ -th iteration can be chosen as

$$\begin{aligned} S_{k,\max}^{\text{lb1}}[n] &\triangleq P_{\text{peak}} \gamma_0 \left( -\frac{(r_{l+1} - \check{b}_k[n])^2}{\check{A}_k^2[n]} + \check{B}_k[n](r_{l+1} - \check{b}_k[n])(r_l - \check{b}_k[n]) + \check{C}_k[n] \right) \\ &\leq S_{k,\max}[n], \forall n, \end{aligned} \quad (35)$$

where the constants  $\check{b}_k[n]$ ,  $\check{A}_k[n]$ ,  $\check{B}_k[n]$ , and  $\check{C}_k[n]$  are respectively given by

$$\begin{aligned} \check{b}_k[n] &\triangleq \zeta_k \cos(\theta[n] - \theta_k), \\ \check{A}_k[n] &\triangleq \zeta_k^2 \sin^2(\theta[n] - \theta_k) + H^2, \\ \check{B}_k[n] &\triangleq 2 \left( \frac{1}{\check{A}_k^2[n]} - \frac{1}{((r_l - \check{b}_k[n])^2 + \check{A}_k[n])^2} \right), \\ \check{C}_k[n] &\triangleq \frac{1}{(r_l - \check{b}_k[n])^2 + \check{A}_k[n]} + \frac{2(r_l - \check{b}_k[n])^2}{((r_l - \check{b}_k[n])^2 + \check{A}_k[n])^2} - \frac{(r_l - \check{b}_k[n])^2}{\check{A}_k^2[n]}. \end{aligned}$$

By applying (15), (P3) for fixed  $\{\theta[n], \omega[n], \alpha[n]\}$  can be reformulated as an approximated convex problem at the  $(l+1)$ -th iteration of the SCA

$$(P3.1) : \max_{\{r_{l+1}, S_{k,l+1}[n], \tau^{\text{lb1}}\}} \tau^{\text{lb1}} \quad (36a)$$

$$s.t. \quad \frac{1}{N} \sum_{n=1}^N \left( \log_2 \left( 1 + \sum_{m=1}^K S_{m,l+1}[n] \right) - \check{R}_k^{\text{ub}}[n] \right) \geq \tau^{\text{lb1}}, \forall k, \quad (36b)$$

$$0 \leq S_k[n] \leq S_{k,\max}^{\text{lb1}}[n], \forall k, n, \quad (36c)$$

$$(10d), (31b),$$

where  $\check{R}_k^{\text{ub}}[n] \triangleq \check{\Gamma}_k[n] \left( \sum_{j=1, j \neq k}^K (S_{j,l+1}[n] - S_{j,l}[n]) \right) + \log_2 \left( 1 + \sum_{j=1, j \neq k}^K S_{j,l}[n] \right)$  and  $\check{\Gamma}_k[n] \triangleq \frac{\log_2 e}{1 + \sum_{j=1, j \neq k}^K S_{j,l}[n]}$ . (P3.1) can be successively solved by the CVX until convergence.

Next, we present a solution for (P3) with a given  $r$ . To obtain the concave surrogate function of  $S_{k,\max}[n]$ , we introduce the following lemma which identifies the surrogate function of the cosine function.

*Lemma 3:* For any given  $\phi_l$ , the concave surrogate function of  $\cos \phi$  can be computed as

$$\frac{-(\phi - \phi_l + \sin \phi_l)^2}{2} + \cos \phi_l + \frac{\sin^2 \phi_l}{2} \leq \cos \phi. \quad (37)$$

*Proof:* With a similar process in Appendix A, we can conclude that the function in (37) satisfies the conditions for a concave surrogate function [23].  $\blacksquare$

By inspecting Lemmas 1 and 3, the concave surrogate function  $S_{k,\max}^{\text{lb2}}[n]$  for  $S_{k,\max}[n]$  can be identified as

$$\begin{aligned} S_{k,\max}^{\text{lb2}}[n] &\triangleq P_{\text{peak}} \gamma_0 \left( -\frac{r\zeta_k \left( \theta_{l+1}[n] - \hat{b}_k[n] \right)^2}{\hat{A}_k^2[n]} + \hat{B}_k[n] \sin(\theta_l[n] - \theta_k) \left( \theta_{l+1}[n] - \hat{b}_k[n] \right) + \hat{C}_k[n] \right) \\ &\leq \frac{P_{\text{peak}} \gamma_0}{r\zeta_k \left( \theta_{l+1}[n] - \hat{b}_k[n] \right)^2 + \hat{A}_k[n]} \leq S_{k,\max}[n], \end{aligned} \quad (38)$$

where  $\hat{b}_k[n]$ ,  $\hat{A}_k[n]$ ,  $\hat{B}_k[n]$ , and  $\hat{C}_k[n]$  are given by

$$\begin{aligned} \hat{b}_k[n] &\triangleq \theta_l[n] - \sin(\theta_l[n] - \theta_k), \\ \hat{A}_k[n] &\triangleq r^2 + \zeta_k^2 + H^2 - r\zeta_k \left( 2 \cos(\theta_l[n] - \theta_k) + \sin^2(\theta_l[n] - \theta_k) \right), \\ \hat{B}_k[n] &\triangleq 2r\zeta_k \left( \frac{1}{\hat{A}_k^2[n]} - \frac{1}{\left( r\zeta_k \sin^2(\theta_l[n] - \theta_k) + \hat{A}_k[n] \right)^2} \right), \\ \hat{C}_k[n] &\triangleq \frac{1}{r\zeta_k \sin^2(\theta_l[n] - \theta_k) + \hat{A}_k[n]} + \frac{2r\zeta_k \sin^2(\theta_l[n] - \theta_k)}{\left( r\zeta_k \sin^2(\theta_l[n] - \theta_k) + \hat{A}_k[n] \right)^2} - \frac{r\zeta_k \sin^2(\theta_l[n] - \theta_k)}{\hat{A}_k^2[n]}. \end{aligned}$$

By utilizing (15) and (38), at the  $(l + 1)$ -th iteration of the SCA algorithm with a given  $r$ , (P3) can be approximated to the following convex problem.

$$(P3.2) : \max_{\substack{\{\theta_{l+1}[n], \omega[n], \alpha[n]\} \\ \{S_{k,l+1}[n], \tau^{\text{lb}2}\}}} \tau^{\text{lb}2} \quad (39a)$$

$$s.t. \quad \frac{1}{N} \sum_{n=1}^N \left( \log_2 \left( 1 + \sum_{m=1}^K S_{m,l+1}[n] \right) - \check{R}_k^{\text{ub}}[n] \right) \geq \tau^{\text{lb}2}, \forall k, \quad (39b)$$

$$0 \leq S_k[n] \leq S_{k,\max}^{\text{lb}2}[n], \forall k, n, \quad (39c)$$

$$(10d), (25) - (29).$$

We then successively solve (P3.2) by the CVX until convergence. Similar to Algorithm 1, a solution of problem (P3) is obtained by alternately solving (P3.1) and (P3.2) until the objective value converges.

For the EE maximization problem (P4) in the circular trajectory case, we can apply similar methods in Section III-B. Based on (P3.1) and (P3.2), given  $\{\theta[n], \omega[n], \alpha[n]\}$  and  $r$ , (P4) can be transformed into two concave-convex fractional problems. By using Algorithm 2, we can alternately solve these problems until convergence.

### B. Trajectory Initialization

To initialize the proposed algorithms, we employ a simple circular path concept in [12]. First, the initial angular velocity  $\omega_0$  is set to  $\omega_0 = \frac{2\pi}{T}$ , which implies  $\theta_0[n] = 2\pi \frac{n}{N}$ ,  $\forall n$ . Next, the initial radius  $r_0$  is chosen to fulfill the constraints in (4), (5), and (10d), which can be expressed as

$$\frac{V_{\min} T}{2\pi} \leq r_0 \leq \min \left( \frac{V_{\max} T}{2\pi}, \frac{a_{\max}}{\omega_0^2} \right), \quad (40)$$

$$c_1 r_0^3 \omega_0^3 + \frac{c_2}{r_0 \omega_0} + \frac{c_2 r_0 \omega_0^3}{g^2} \leq P_{\text{lim}}. \quad (41)$$

We can simply find  $r_0$  which maximizes the minimum rate in (P1) and (P3) under constraints (40) and (41) via one-dimensional line search. For the EE maximization problems (P2) and (P4),  $r_0$  can be computed in the range of (40). As a result, the initial trajectory  $\mathbf{q}_0[n]$  can be written by  $\mathbf{q}_0[n] = [r_0 \cos 2\pi \frac{n}{N} + x_0 \quad r_0 \sin 2\pi \frac{n}{N} + y_0]^T$  ( $n = 0, 1, \dots, N$ ) and the initial velocity  $\mathbf{v}_0[n]$  can be simply obtained as  $\mathbf{v}_0[n] = (\mathbf{q}_0[n+1] - \mathbf{q}_0[n]) / \delta_t$  ( $n = 0, 1, \dots, N-1$ ) assuming  $\delta_t^2 \approx 0$  in (2).

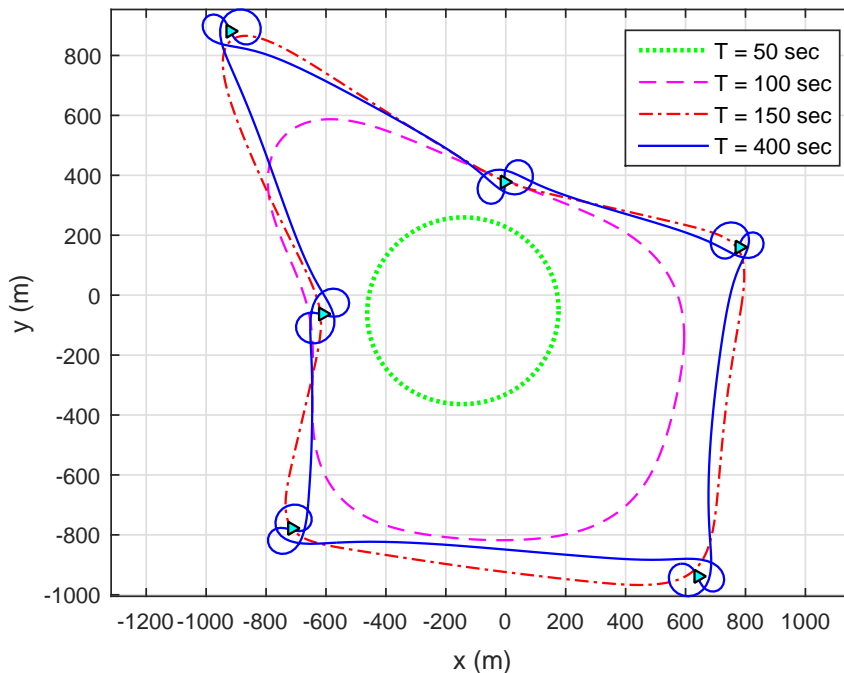


Fig. 2. Optimized UAV trajectories for different periods  $T$  with  $P_{\text{lim}} = 150$  W.

## V. NUMERICAL RESULTS

In this section, we provide numerical results to validate the effectiveness of the proposed algorithms. For the simulations, we consider  $K = 6$  GNs which are distributed as in Fig. 2 where the locations of the GNs are marked with the triangles. The constant altitude, the bandwidth, the reference SNR, and the peak transmission power are set to be  $H = 100$  m,  $W = 1$  MHz,  $\gamma_0 = 80$  dB, and  $P_{\text{peak}} = 10$  dBm, respectively. Also, the minimum velocity, the maximum velocity, and the maximum acceleration of the UAV are determined as  $V_{\text{min}} = 3$  m/sec,  $V_{\text{max}} = 100$  m/sec, and  $a_{\text{max}} = 5$  m/sec<sup>2</sup>, respectively. For the propulsion power consumption model in (6), the constants  $c_1$  and  $c_2$  are set as  $c_1 = 9.26 \times 10^{-4}$  and  $c_2 = 2250$ , respectively, which make the minimum propulsion power consumption  $P_{\text{prop,min}} = 100$  W when  $\|\mathbf{v}\| = 30$  m/sec.

We first demonstrate the performance of the minimum rate maximization algorithms. Fig. 2 illustrates the optimized UAV trajectories with various  $T$  for  $P_{\text{lim}} = 150$  W. It is observed that when  $T$  is smaller than 150 sec, as  $T$  increases, the UAV tries to get closer to all GNs in order to improve the channel conditions from the GNs. In contrast, if  $T$  is sufficiently large ( $T = 400$  sec), the UAV is now able to visit all the GNs within a given time period. Thus, the UAV can



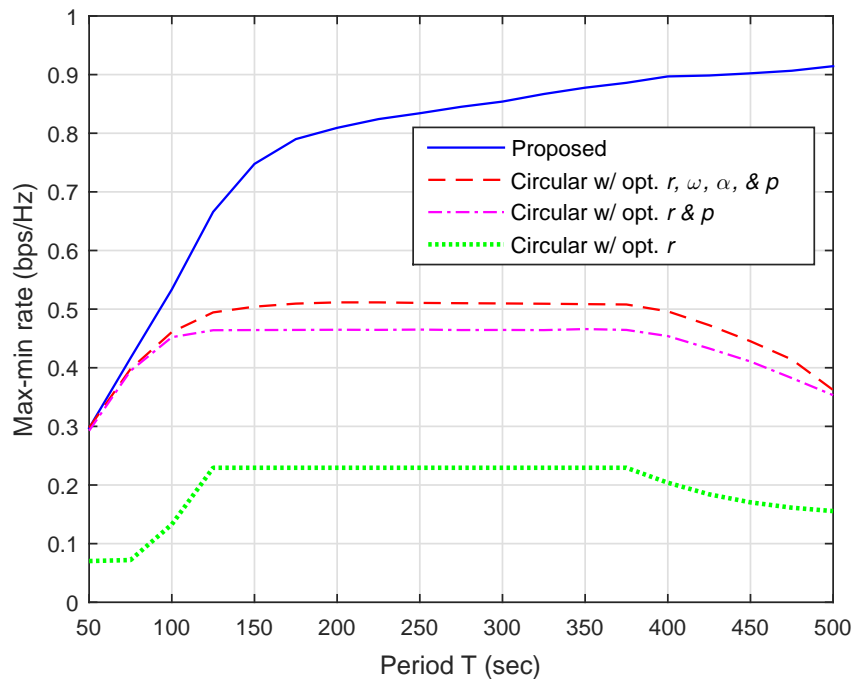


Fig. 3. Max-min rate with respect to the period  $T$  with  $P_{\text{lim}} = 150$  W.

hover over each GN for a while by traveling smooth path around the GNs. This is different from the results in [12] where the UAV does not have practical movement constraints. This can be explained as follows: Due to the constraints on the velocity and the propulsion power, the UAV cannot stay at fixed positions as in [12]. Therefore, the UAV continuously moves around as close to the GNs as possible to maintain good communication channels without exceeding the propulsion power limit  $P_{\text{lim}}$ .

Fig. 3 shows the maximized minimum (max-min) rate performance of the proposed algorithm as a function of  $T$ . We compare the performance of the proposed algorithm with the following circular trajectory based methods.

- *Circular with optimum  $r, \omega, \alpha, \text{ and } p$* : radius, angular velocity, angular acceleration, and uplink transmit power are jointly optimized with (P3) in Section IV-A with the circular trajectory.
- *Circular with optimum  $r$  and  $p$* : radius and uplink transmit power are jointly optimized with (P3.1) in Section IV-A with the circular trajectory.
- *Circular with optimum  $r$* : radius is optimized with  $P_{\text{peak}}$  as the initial circular trajectory in

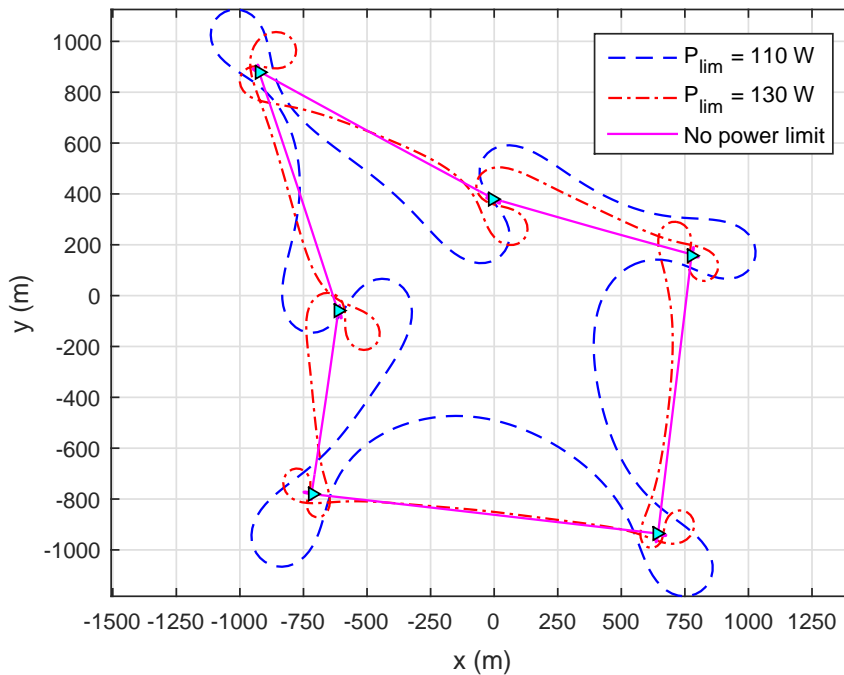


Fig. 4. Optimized UAV trajectories for different propulsion power limit  $P_{lim}$  with  $T = 400$  sec.

#### Section IV-B

First, it can be verified that the proposed algorithm outperforms the baseline schemes regardless of the time period  $T$ . Also, we can see that the max-min rate in the proposed algorithm monotonically increases with  $T$ , since more time is available at the UAV to hover around each GN. In contrast, in the baseline schemes which are restricted in circular shape trajectory, the max-min rate performance first increases as  $T$  grows, and then decreases after a certain  $T$ . This is due to a fact that in order to satisfy the propulsion power constraint, the radius of the circular trajectory should increase as  $T$  gets large, and thus the UAV may become too far away from the geometric center of the GNs after a certain  $T$ . Therefore, we can expect the performance gain of the proposed algorithm over baseline schemes is to grow with  $T$ .

Fig. 4 illustrates the optimized UAV trajectories for various propulsion power limit  $P_{lim}$  with  $T = 400$  sec. It can be shown that for  $P_{lim} = 110$  W, the trajectory of the UAV is restricted to a smooth path with a large turning radius to consume a low propulsion power. However, as  $P_{lim}$  gets larger, we observe quick changes along the trajectory path. Thus the UAV can move with a much smaller turning radius, which enhances the max-min rate performance.

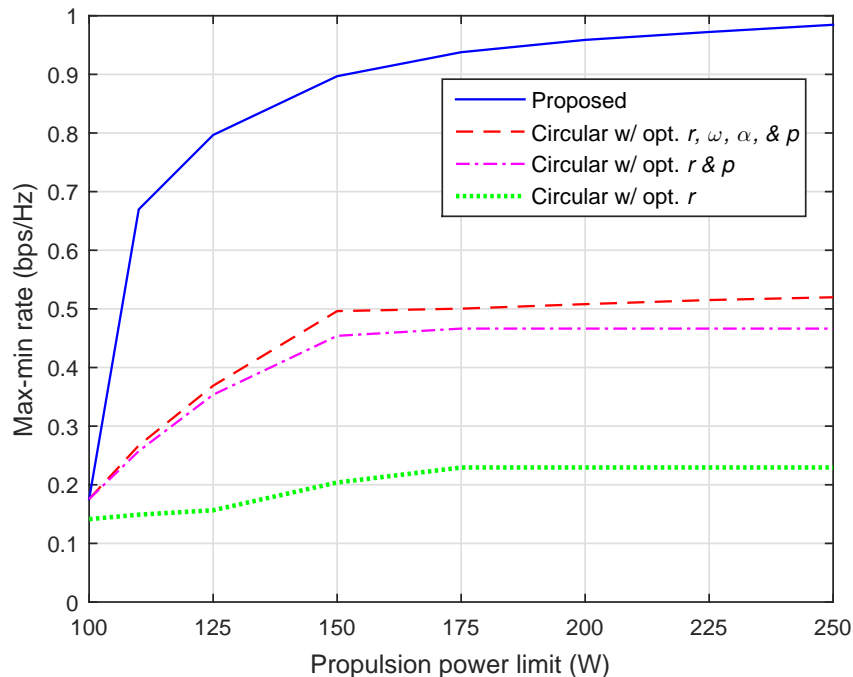


Fig. 5. Max-min rate with respect to the propulsion power limit  $P_{\text{lim}}$  with  $T = 400$  sec.

In Fig. 5, we depict the average max-min rate of various schemes as a function of the propulsion power constraint  $P_{\text{lim}}$ . For both the proposed algorithm and the baseline schemes, the max-min rate first increases as  $P_{\text{lim}}$  grows and then gets saturated. This can be explained as follows: With a large  $P_{\text{lim}}$ , the trajectory and the velocity of the UAV change more freely to attain good channel conditions, and thus the max-min rate increases. However, even if a large  $P_{\text{lim}}$  is given, the max-min rate cannot continue to increase because there are practical limits on the velocity and acceleration. Similar to Fig. 3, we can see that the proposed algorithm provides significant performance gains over the baseline schemes.

Next, in Fig. 6, we investigate the optimized trajectory of the EE maximization problem with various  $T$ . As  $T$  increases, the overall patterns are similar to Fig. 2. Nevertheless, to balance between the rate performance and the propulsion power consumption, the EE maximization trajectory shows a smooth path with a relatively large turning radius, and thus the average propulsion power consumption becomes lower.

To present the impact of the energy efficient UAV communication designs, Fig. 7 depicts the UAV speed of the proposed EE maximization method with  $T = 400$  sec. For comparison, we

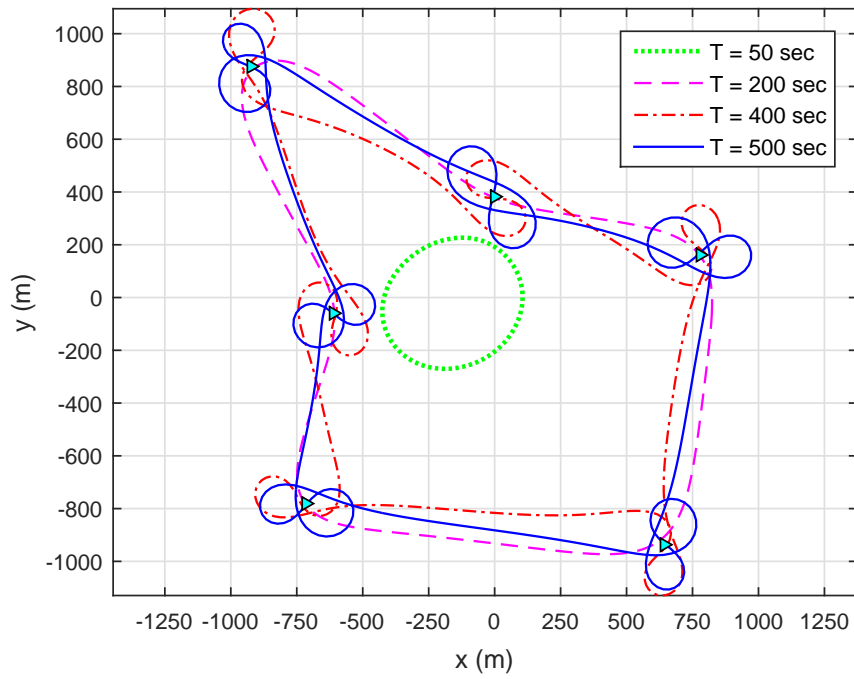


Fig. 6. Optimized energy efficient UAV trajectories for different periods  $T$

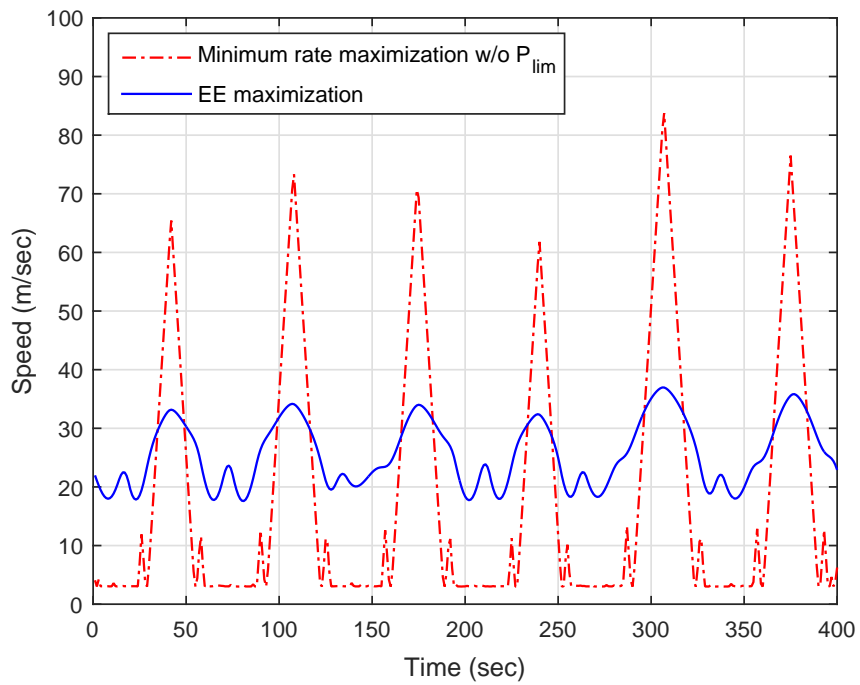


Fig. 7. UAV speeds for the max-min rate without propulsion power constraint and the EE maximization with  $T = 400$  sec

TABLE I  
PERFORMANCE COMPARISON WITH MAX-MIN RATE AND EE MAXIMIZATION FOR  $T = 400$  SEC

		Average speed (m/sec)	Average acceleration (m/sec <sup>2</sup> )	Average max-min rate (bps/Hz)	Average power (Watts)	Energy efficiency (kbits/Joule)
Max-min rate w/o $P_{lim}$	Proposed	18.42	4.73	0.99	553.01	1.80
	Circular	13.50	1.88	0.53	541.41	0.98
EE maximization	Proposed	25.73	2.71	0.79	122.14	6.47
	Circular	15.35	0.27	0.47	151.33	3.10

also consider the max-min rate scheme without the propulsion power constraint. It is observed that for the max-min rate case, the UAV tries to fly between the GNs as fast as possible and stay over the GNs with a low speed. On the other hand, the EE maximization scheme keeps the speed of the UAV at around 30 m/sec in order not to waste the propulsion energy.

Finally, Table I presents the performance comparison of the max-min rate without propulsion power constraint and the EE maximization designs for both the proposed and the baseline schemes with  $T = 400$  sec. We can see that the max-min rate methods consume much higher propulsion power by allowing a large variation of the speed and the average acceleration. In contrast, the speed of the proposed EE maximization design slowly varies with low acceleration, and thus much higher EE can be achieved. We observe that the proposed EE maximization algorithm exhibits about 259 % gain over the max-min rate without the propulsion power constraint and 109 % gain over the circular baseline EE maximization scheme.

## VI. CONCLUSION

In this paper, we have studied the UAV-aided wireless communication optimization under the practical propulsion energy constraint at the UAV. For both the minimum average rate maximization problem and the EE maximization problem, the UAV trajectories and the uplink transmit power of the GNs have been jointly optimized. By applying the SCA technique, we have proposed efficient iterative algorithms which find local optimal solutions. Numerical results have demonstrated that the proposed algorithms provide substantial performance gains compared to the baseline schemes.

## APPENDIX A

## PROOF OF LEMMA 1

Let us define a function  $f_1(\mathbf{u}) \triangleq \frac{1}{\rho\|\mathbf{u}\|^2+z}$  for  $\mathbf{u} = [u_x \ u_y]^T$  where  $z$  and  $\rho$  are positive constants. For any given  $\mathbf{u}_l \in \mathbb{R}^{2 \times 1}$ , in order for arbitrary function  $g_1(\mathbf{u}|\mathbf{u}_l)$  to be a concave surrogate function of  $f_1(\mathbf{u})$ , it must satisfy the following conditions:  $f_1(\mathbf{u}_l) = g_1(\mathbf{u}_l|\mathbf{u}_l)$ ,  $\nabla g_1(\mathbf{u}_l|\mathbf{u}_l) = \nabla f_1(\mathbf{u}_l)$ , and  $g_1(\mathbf{u}|\mathbf{u}_l) \leq f_1(\mathbf{u})$ ,  $\forall \mathbf{u}$  [23]. Denoting the function  $g_1(\mathbf{u}|\mathbf{u}_l)$  as

$$g_1(\mathbf{u}|\mathbf{u}_l) \triangleq -\frac{\rho\|\mathbf{u}\|^2}{z^2} + \overline{B}\mathbf{u}^T\mathbf{u}_l + \overline{C}, \quad (42)$$

where  $\overline{B} \triangleq 2\rho\left(\frac{1}{z^2} - \frac{1}{(\rho\|\mathbf{u}_l\|^2+z)^2}\right)$  and  $\overline{C} \triangleq \frac{1}{\rho\|\mathbf{u}_l\|^2+z} + \frac{2\rho\|\mathbf{u}_l\|^2}{(\rho\|\mathbf{u}_l\|^2+z)^2} - \frac{\rho\|\mathbf{u}_l\|^2}{z^2}$ , it can be easily shown that  $f_1(\mathbf{u}_l) = g_1(\mathbf{u}_l|\mathbf{u}_l)$ , i.e.,  $g_1(\mathbf{u}|\mathbf{u}_l)$  fulfills the first condition for the surrogate function.

Also, the gradient of  $f_1(\mathbf{u})$  and  $g_1(\mathbf{u}|\mathbf{u}_l)$  with respect to  $\mathbf{u}$  can be respectively computed as

$$\nabla f_1(\mathbf{u}) = -\frac{-2\rho\mathbf{u}}{(\rho\|\mathbf{u}\|^2+z)^2}, \quad (43)$$

$$\nabla g_1(\mathbf{u}|\mathbf{u}_l) = -\frac{2\rho\mathbf{u}}{z^2} + \overline{B}\mathbf{u}_l. \quad (44)$$

Since two gradients in (43) and (44) become identical at  $\mathbf{u} = \mathbf{u}_l$ ,  $g_1(\mathbf{u}|\mathbf{u}_l)$  satisfies the second condition for the surrogate function.

To prove the global lower bound condition, we can calculate the Hessian matrix  $\nabla_{\mathbf{u}}^2 h_1(\mathbf{u}|\mathbf{u}_l)$  of the function  $h_1(\mathbf{u}|\mathbf{u}_l) \triangleq f_1(\mathbf{u}) - g_1(\mathbf{u}|\mathbf{u}_l)$  as

$$\nabla^2 h_1(\mathbf{u}|\mathbf{u}_l) = D \begin{bmatrix} E + 4\rho z^2 u_x^2 & 4\rho z^2 u_x u_y \\ 4\rho z^2 u_x u_y & E + 4\rho z^2 u_y^2 \end{bmatrix}, \quad (45)$$

where  $D \triangleq \frac{2\rho}{z^2(\rho\|\mathbf{u}\|^2+z)^3} > 0$  and  $E \triangleq \rho^3\|\mathbf{u}\|^6 + 3\rho^2 z\|\mathbf{u}\|^4 + 2\rho z^2\|\mathbf{u}\|^2 \geq 0$ . One can easily check that the Hessian in (45) is a positive semi-definite matrix, which implies that  $h_1(\mathbf{u}|\mathbf{u}_l)$  is a convex function.

Since  $\nabla h_1(\mathbf{u}|\mathbf{u}_l) = \mathbf{0}$  at  $\mathbf{u} = \mathbf{u}_l$  from (43) and (44), the global minimum of  $h_1(\mathbf{u}|\mathbf{u}_l)$  is achieved at  $\mathbf{u} = \mathbf{u}_l$  with  $h_1(\mathbf{u}_l|\mathbf{u}_l) = 0$ . As a result, we can show that  $h_1(\mathbf{u}|\mathbf{u}_l)$  is greater than or equal to 0 for any given  $\mathbf{u}_l$ , and thus the third condition for the surrogate function holds. By substituting  $\mathbf{u} = \mathbf{q}_{l+1}[n] - \mathbf{w}_k$ ,  $\mathbf{u}_l = \mathbf{q}_l[n] - \mathbf{w}_k$ ,  $z = H^2$ , and  $\rho = 1$  and multiplying  $f_1(\mathbf{u})$  and  $g_1(\mathbf{u}|\mathbf{u}_l)$  by  $P_{\text{peak}}\gamma_0$ , Lemma 1 is thus proved.

## REFERENCES

- [1] Y. Zeng, R. Zhang, and T. J. Lim, "Wireless communications with unmanned aerial vehicles: opportunities and challenges," *IEEE Commun. Mag.*, vol. 54, pp. 36–42, May. 2016.

- [2] W. Lee, I. Lee, J. S. Kwak, B.-C. Ihm, and S. Han, "Multi-BS MIMO cooperation: challenges and practical solutions in 4G systems," *IEEE Wireless Commun.*, vol. 19, pp. 89–96, Feb. 2012.
- [3] Y. Zeng, R. Zhang, and T. J. Lim, "Throughput maximization for UAV-enabled mobile relaying systems," *IEEE Trans. Commun.*, vol. 64, pp. 4983–4996, Dec. 2016.
- [4] Q. Wang, Z. Chen, W. Mei, and J. Fang, "Improving physical layer security using UAV-enabled mobile relaying," *IEEE Wireless Commun. Lett.*, vol. 6, pp. 310–313, Jun. 2017.
- [5] C. Song, K.-J. Lee, and I. Lee, "Designs of MIMO amplify-and-forward wireless relaying networks: challenges and solutions," *IEEE Access*, vol. 5, pp. 9223–9234, May. 2017.
- [6] H.-B. Kong, C. Song, H. Park, and I. Lee, "A new beamforming design for MIMO AF relaying systems with direct link," *IEEE Trans. Commun.*, vol. 62, pp. 2286–2295, Jul. 2014.
- [7] A. Merwaday and I. Guvenc, "UAV assisted heterogeneous networks for public safety communications," in *Proc. IEEE WCNC*, pp. 329–334, May. 2015.
- [8] J. Lyu, Y. Zeng, and R. Zhang, "Spectrum sharing and cyclical multiple access in UAV-aided cellular offloading," *arXiv preprint arXiv:1705.09024*, 2017.
- [9] S. Jeong, O. Simeone, and J. Kang, "Mobile edge computing via a UAV-mounted cloudlet: optimization of bit allocation and path planning," *accepted in IEEE Trans. Veh. Technol.* [Online] Available: <http://arxiv.org/abs/1609.05362>.
- [10] A. Al-Hourani, S. Kandeepan, and S. Lardner, "Optimal LAP altitude for maximum coverage," *IEEE Wireless Commun. Lett.*, vol. 3, pp. 569–572, Jul. 2014.
- [11] J. Lyu, Y. Zeng, and R. Zhang, "Cyclical multiple access in UAV-aided communications: a throughput-delay tradeoff," *IEEE Wireless Commun. Lett.*, vol. 5, pp. 600–603, Dec. 2016.
- [12] Q. Wu, Y. Zeng, and R. Zhang, "Joint trajectory and communication design for multi-UAV enabled wireless networks," *arXiv:1705.02723*, 2017.
- [13] A. Filippone, *Flight performance of fixed and rotary wing aircraft*. Elsevier, 2006.
- [14] D. H. Choi, S. H. Kim, and D. K. Sung, "Energy-efficient maneuvering and communication of a single UAV-based relay," *IEEE Trans. Aerosp. Electron. Syst.*, vol. 50, pp. 2320–2327, Jul. 2014.
- [15] J. Zhang, Y. Zeng, and R. Zhang, "Spectrum and energy efficiency maximization in UAV-enabled mobile relaying," in *Proc. IEEE ICC*, pp. 1–6, May. 2017.
- [16] Y. Zeng and R. Zhang, "Energy-efficient UAV communication with trajectory optimization," *IEEE Trans. Wireless Commun.*, vol. 16, pp. 3747–3760, Jun. 2017.
- [17] H. Kim, S.-R. Lee, C. Song, K.-J. Lee, and I. Lee, "Optimal power allocation scheme for energy efficiency maximization in distributed antenna systems," *IEEE Trans. Commun.*, vol. 63, pp. 431–440, Feb. 2015.
- [18] J. Xu and L. Qiu, "Energy efficiency optimization for MIMO broadcast channels," *IEEE Trans. Wireless Commun.*, vol. 12, pp. 690–701, Feb. 2013.
- [19] S.-R. Lee, J. Jung, H. Park, and I. Lee, "A new energy-efficient beamforming strategy for MISO interfering broadcast channels based on large systems analysis," *IEEE Trans. Wireless Commun.*, vol. 15, pp. 2872–2882, Apr. 2016.
- [20] B. Du, C. Pan, W. Zhang, and M. Chen, "Distributed energy-efficient power optimization for CoMP systems with max-min fairness," *IEEE Commun. Lett.*, vol. 18, pp. 999–1002, Jun. 2014.
- [21] Y. Li, M. Sheng, C. W. Tan, Y. Zhang, Y. Sun, X. Wang, Y. Shi, and J. Li, "Energy-efficient subcarrier assignment and power allocation in OFDMA systems with max-min fairness guarantees," *IEEE Trans. Commun.*, vol. 63, pp. 3183–3195, Sep. 2015.
- [22] Y. Li, M. Sheng, X. Wang, Y. Zhang, and J. Wen, "Max-min energy-efficient power allocation in interference-limited wireless networks," *IEEE Trans. Veh. Technol.*, vol. 64, pp. 4321–4326, Sep. 2015.

- [23] B. R. Marks and G. P. Wright, "A general inner approximation algorithm for nonconvex mathematical programs," *Operations Research*, vol. 26, pp. 681–683, Aug. 1978.
- [24] Y. Sun, P. Babu, and D. P. Palomar, "Majorization-minimization algorithms in signal processing, communications, and machine learning," *IEEE Trans. Signal Process.*, vol. 65, pp. 794–816, Feb. 2017.
- [25] M. Grant and S. Boyd, "CVX: Matlab software for disciplined convex programming, version 2.1." Available: <http://cvxr.com/cvx>, 2017.
- [26] W. Dinkelbach, "On nonlinear fractional programming," *Management science*, vol. 13, pp. 492–498, Mar. 1967.
- [27] A. Zappone and E. Jorswieck, "Energy efficiency in wireless networks via fractional programming theory," *Foundations and Trends in Communications and Information Theory*, vol. 11, pp. 185–396, Jun. 2015.